Cathode Spots Dynamics in a High-Current Vacuum Arc Thruster: Aluminum vs Iron

Etienne Michaux, Stéphane Mazouffre, Julien Jérémie

Cathode spots dynamics in a high-current Vacuum Arc Thruster: Aluminum vs iron

Etienne Michaux* and Stéphane Mazouffre†
Institut de Combustion, Aérothermique, Reactivité et Environnement (ICARE) - CNRS, Orléans, 45071, France

Jérémie Julien‡
Institut Polytechnique des Sciences Avancées (IPSA), Ivry-sur-Seine, 94200, France

This study investigates the apparent motion of cathode spots in a 30 W vacuum arc thruster by means of high-speed imaging. Images taken at 450,000 frames per second allowed to observe the evolution of cathode spots distribution throughout a single single discharge. Experiments were conducted with two different cathode materials: aluminum and iron. Associating the images and the discharge current reveals regions of high local current density, reaching approximately 10^9 A/m^2. Examining patterns in cathode spot clustering and mapping their trajectories lead to valuable insights into cathode erosion dynamics.

I. Nomenclature

I_d = discharge current
j = current density
r_s = Spearman rank order coefficient
S = spot surface
σ = standard deviation
v = spot apparent velocity

II. Introduction

The vacuum arc thruster (VAT) is an electric space thruster that creates an electrical arc. Contrary to what happens at atmospheric pressure, in vacuum there is no medium to ionize. The electrode where the lowest potential is applied, the cathode, is vaporized and ionized. The ejected plasma generates a thrust in the opposite direction. The VAT is a simple and robust thruster, thus a good choice for micro-propulsion applications. In addition, the storage density is high and there is no need for any fluid management system or tank.

However, the vacuum arc is a complex and highly dynamic phenomenon. On rather small time scales, plasma properties change and the plasma emission sites move over the cathode surface [1]. Their study is then difficult, and some aspects of the vacuum arc behavior remain unclear despite more than 70 years of research effort [2, 3]. Most recent research works highlight the fractal nature of cathode spots [4], which are the plasma emission sites at the cathode surface. This nature is reflected both in the way the spots are distributed on the cathode surface, and in the voltage fluctuations noise at the electrodes [5]. In other words, the vacuum arc shows a high complexity both in the spatial and in the temporal domain.

In the context of VATs, the arc is pulsed with a short duration in order to avoid thermal issues. A study on the arc dynamics is then of high importance. In particular, knowledge on the cathode spots distribution throughout the discharge duration is of major interest when it comes to engineering considerations. In fact, VATs suffer from performance limitations due to the random nature of the cathode erosion. In this study, the time evolution of cathode spots that cover the surface is investigated by means of high-speed imaging. Measurements are performed with a 30-W VAT that has the particularity of operating a very high current, in the magnitude of kiloamperes. The clustering mechanism of plasma emission sites is observed in the context of a high-current VAT, as well as the spots current density for two different cathode materials. Ultimately, the propagation speed of the spot structure is determined and conclusions are drawn.

*PhD Student, ICARE - CNRS, 1c Av. de la recherche scientifique, 45071, Orléans, France
†Research Director, ICARE - CNRS, 1c Av. de la recherche scientifique, 45071, Orléans, France
‡Graduate Student, IPSA, 63 Bd de Brandebourg, 94200, Ivry-sur-Seine, France

III. Experimental arrangement

A. The Plasma Jet Pack

The Plasma Jet Pack (PJP) is a high-current Vacuum Arc Thruster (VAT) developed by the COMAT french company. Several PJP versions have been developed to date, for different needs and different satellite integrations[6]The PJP under study is the H2020 version, designed to be easily dismountable which allows testing of different electrode configurations. In particular, this version can be equipped with cathodes made out of different materials. The PJP generates a high-current vacuum arc through the cyclic discharges of a capacitor bank. The repetition frequency can reach 2 Hz at maximum, for a power consumption of 30 W. The cathode to anode voltage is continuously set to 250 V. A triggering system applies a few kV pulse on the cathode surface for 1 µs. This pulse allows ignition of the plasma through an explosive process [7] . The cathode material is locally vaporized and ionized, on surface regions called cathode spots. After the trigger is switched-off, the arc is forced to propagate to the anode through the existing metal vapor. This second arc discharge allows roughly 2.5 to 4 kA to flow between the two electrodes with the present configuration, depending on the cathode material. Overall, the energy released over 30 µs into one single PJP discharge reaches more or less 3 J. Measurements presented in this work have been conducted with a copper anode and two different cathode materials: iron and aluminum. Averaged PJP discharge current waveforms (I_d) are given in Fig. 1a, over the whole dataset, for iron and aluminum cathodes. Despite slight differences in the maximum current from one pulse to an other, the temporal evolution of the discharge current remains the same for a given cathode material. In brief the I_d waveforms are highly reproducible for a given cathode material.

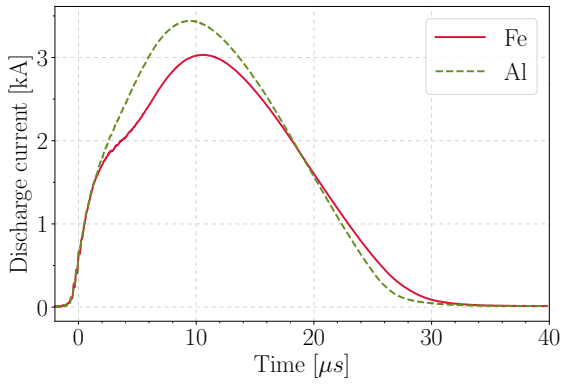

(a) Typical PJP discharge current waveform during one pulse, with Fe and Al cathodes.

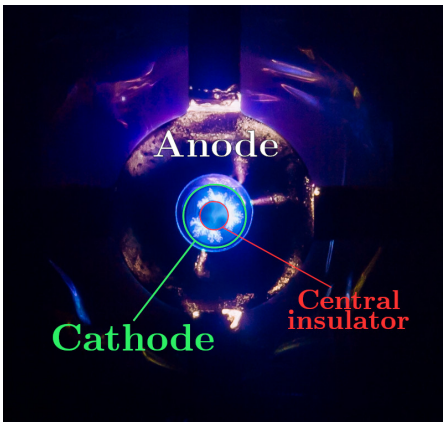

(b) PJP thruster during operation: front view. The bright patterns seen on the cathode are the cathode spots. © Cyril FRESILLON / ICARE / CNRS Images.

Fig. 1 PJP thruster front view and averaged discharge current waveforms.

Figure 1b shows a front view of the PJP during operation. The larger circular electrode is the anode. The cathode, circled in green on the figure, is a hollow cylinder screwed onto a copper plate directly connected to the capacitor bank. The middle of this cylinder contains an insulator, circled in red, designed to separate the cathode from the discharge triggering system. The latter is a tiny electrode placed exactly on the thruster axis of symmetry, which applies a high voltage over a very short period of time allowing a breakdown that initiates the discharge. The gap in the axial direction between the cathode and the anode is approximately 1 cm. The cathode spots are here the bright branches that develop on the cathode surface. The central insulator is dark in this picture as the spots develop solely on the cathode surface. The PJP target performance and characteristics are given in Table 1 for the inclined reader.

B. EPIC-2 vacuum chamber

Experiments have been performed in the EPIC-2 vacuum chamber. This tank is a stainless steel cylinder 54 cm in diameter and 104 cm in length, for an approximate capacity of 240 L. Two 2200 L/s (N_2) magnetically levitated Edwards STP-iS2207 are placed on top of the chamber, see Fig. 2. Those pumps evacuated through a 110 m^3/h dry primary pump (Edwards GV110), permit to keep a background pressure of 10^{-6} mbar during thruster operation. The

Table 1 PJP thruster target performance and characteristics.

Power	0-30	W
Thrust to power	10	µN/W
Average thrust at 30 W	300	µN
Specific impulse	2500	s
Total impulse	400	N s
Overall mass	1	kg
Overall volume	1	U

pressure is monitored with a Pfeiffer PBR260 Pirani/Payard-Alpert pressure gauge.

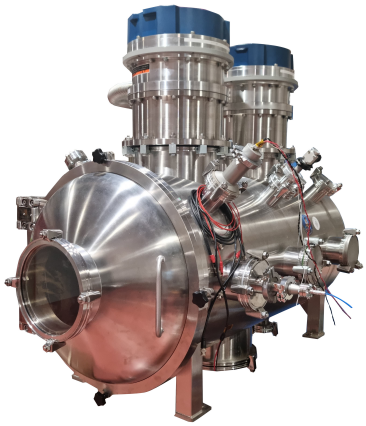

Fig. 2 EPIC-2 vacuum chamber.

EPIC-2 is also equipped with several electrical feedthroughs, for both in-situ diagnostics and thruster power supply. Those feedthroughs are mostly composed of BNC or SubD connectors. Two Kodial (Borosilicate 7056) glass windows allow the visual inspection of the thruster during operation. Inside the chamber, the PJP is mounted on a square fixed to a plate, the latter being screwed on rails. This mounting allows adjustments of the distance to the windows or to instruments, depending on the experiment to be performed.

C. High-speed imaging

It was shown in ref [8] that the spot distribution strongly varies from one pulse to an other. This chaotic nature of vacuum arc [4, 5] requires examination on a pulse-by-pulse basis. Therefore, the use of a high-speed camera is necessary for studying the spots motion dynamics. In this context, the Phantom TMX7510 camera was the best available option. It features a CMOS sensor with an acquisition frequency of up to 1.7 million frames per second (fps). However, at this rate, the image resolution has to be lowered to 256x32 px. To ensure all the cathode surface is contained in the image and that no spot initiates out of the frame, the image resolution is set in this study to 256x128 px. This resolution leads to an acquisition frequency of 450,000 fps, which represents roughly one picture every 2.2 µs. With these settings, 13 photographs are captured throughout a single PJP discharge.

The camera captures footage of the thruster from outside the chamber, through a quartz window. To enhance observational capabilities, a Nikon 200 mm lens is mounted on the camera. This enable zooming on the cathode surface, so that it fills the entire camera field of view. For the same reason, the PJP is placed 30 cm away from the window, which is the closest possible position. Overall, the camera lens is positioned 90 cm away from the cathode, on a stainless steel stand. Due to the large amount of light emitted during the discharges, 2 neutral density filters are installed upstream of the lenses. These filters have a respective optical density of 1 and 2, ensuring that the camera sensor is not saturated. Such saturation would result in a loss of information in the acquired images.

IV. Methodology

In order to compare this study with previous results obtained with this VAT [8] , a series of 30 pulses is performed prior to measurements. These pulses are used to remove the oxide layer formed on the cathode, which modifies the behavior of the vacuum arc [9–11] . To ensure the best possible level of detail, focus is achieved by setting the camera's exposure time to 10 ms, its maximum. This increases the image brightness when no arc is triggered, thus facilitating manual focusing. A calibration image is taken after focusing, and used as a reference for automatic cathode edge detection as it will be explained later. For video acquisition, the exposure time is reduced to 1.9 µs, which is as close as possible to the acquisition period of 2.2 µs. This limits the loss of information between 2 images. The camera is triggered by the PJP trigger signal, the associated discharge current is recorded on the oscilloscope. 150 associations of videos and discharge current were recorded for both cathode materials. Example of a video taken with the aluminum cathode is shown in Fig 3a, and with a Fe cathode in Fig. 3b. In this study, these two videos will serve as references for the various figures representing the analysis of a single pulse.

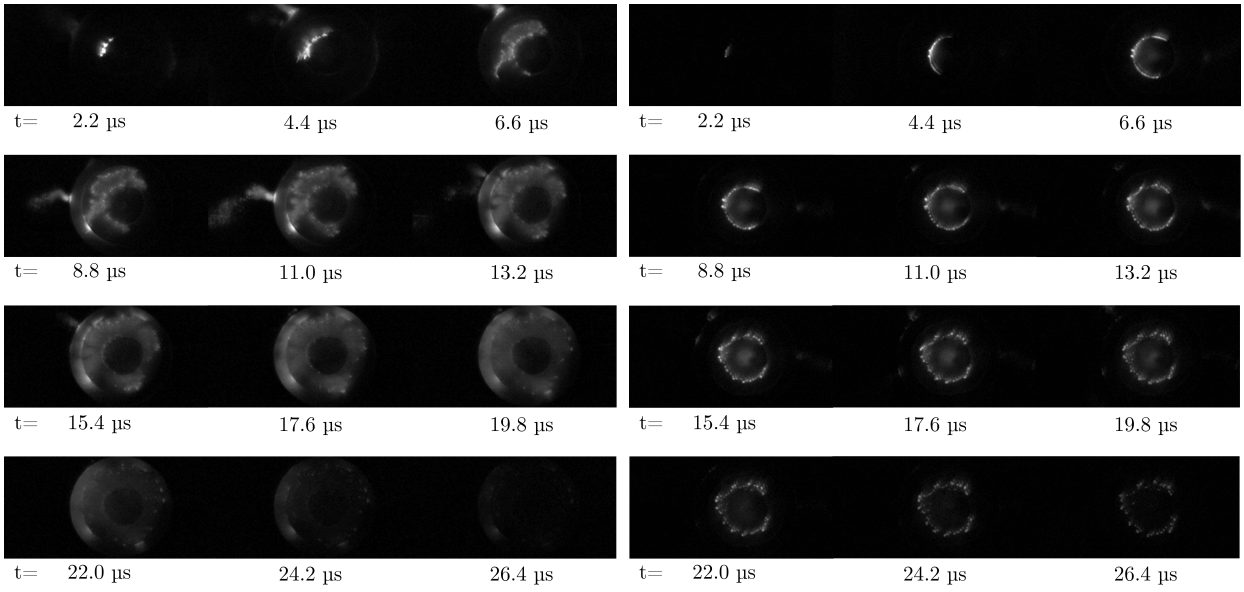

(a) PJP discharge with aluminum cathode

(b) PJP discharge with iron cathode

Fig. 3 12 main frames composing a video, for the two different cathode materials.

Data analysis algorithms are based here on OpenCV. This computer vision library incorporates functions for image processing. Hence, it enables the automatic treatment of a large volume of images. In our study, OpenCV is used to determine cathode edges on all the videos. Due to the geometry of the PJP H2020, an arc can form on the side of the cathode or present anodic modes. Although these phenomena are fairly rare, these luminous areas must not be confused with cathode spots, as this could distort the result when calculating the mean surface covered by the spots or their propagation speed. The cathode edge determination is then an important prerequisite for further rigorous analysis.

For a pixel to be identified as a cathode spot, its brightness must exceed a given threshold. This threshold is set according to the cathode material, as the elements emits at different wavelengths, with different intensities. For example, the threshold for aluminum has been set at 78% of the maximum pixel intensity (200/255), while for iron it's 94% (240/255). These values are obviously not absolute, and are empirically adapted to our datasets and optical equipment. For example, it is clear from Fig. 3 that aluminum has less bright cathode spots than iron, hence the different threshold. It is important to correctly set it since the spots produce a lot of light, illuminating the cathode surface. The spots are a primary source of light and the cathode itself is a secondary source, not an active plasma emission site. Reflected light should not be counted as a cathode spot, to reduce inaccuracies on the results.

V. Results

A. Spot surface

On the whole, see Fig. 3, the spots tend to cluster near the center at the beginning of the discharge. This was to be expected, as the HV trigger tip is located at the center of the cathode central insulator (see Fig. 1b). The breakdown is therefore initiated where the electric field is the strongest: i.e close to the trigger tip. As explained in section III.A, once the trigger is switched off the arc migrates toward the main anode. The latter is circular in shape, and its diameter is larger than the outer diameter of the cathode. The electric field **E** is therefore radial on the picture, leading to a predominantly radial propagation of the cathode spots as the arc is attracted to the outside edge. This does not exclude the possibility for the spots to propagate in a tangential direction. The phenomenon is particularly seen in Fig. 3b, with the Fe cathode. It should also be noted that in this figure, propagation around the central insulator is quite symmetrical. Tangential propagation has no preferential direction between the upper and the lower part of the cathode on the pictures. However, the successive ignitions of the spots close to the active ones is clearly seen here [12, 13]. These two videos were selected as examples because the discharge initiates at approximately the same location. However, from the second frame onward, distinct behaviors can be observed depending on the material. While for aluminum the spots tends to develop radially, rapidly spreading, iron spots remains concentrated around the central insulator. Additionally, the aluminum spots exhibit lower brightness intensity and appear to extinguish more quickly than the iron spots. This difference in behavior is observed regardless of the discharge, aligning with findings from previous studies [8, 14]

On another matter, the total surface covered by the spots shows a significant evolution during the discharge. As spots propagate towards the outside edge, they cover an increasingly larger surface. Figure 4 presents a comparison between the discharge current and the evolution of the covered area as a function of time, for the two videos in Fig. 3. The 13 points between 0 and 28 µs on the graphs correspond to the frames composing Fig 4. The maximum surface is reached when the discharge current reaches its maximum, then it decreases and falls back to zero. We can see that the 2 curves exhibit a high degree of similarity, which is observed consistently across all recorded videos. In particular, we can see from the 2 examples that the PJP slightly malfunctioned at the start of the discharge but that the evolution of the surface still followed the discharge current waveform. The 2.2 µs offset between the two curves in Fig 4 originates in the time taken by the camera to acquire an image (exposure time).

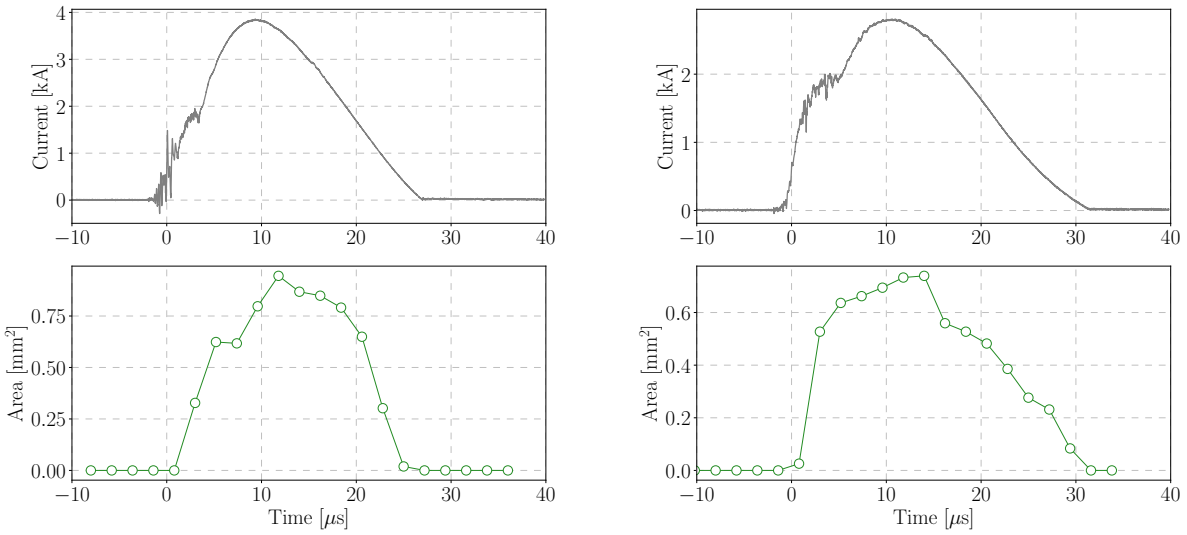

(a) Aluminum cathode, from video shown in Fig. 3a

(b) Iron cathode, from video shown in Fig. 3b

Fig. 4 Comparison between the discharge current (top) and the evolution of the spot surface (bottom) for the two example videos.

The correlation between the discharge current $I_d(t)$ and the surface covered in time $S(t)$ can be quantified by

determining the Spearman rank-order correlation coefficient r_s. This coefficient ranges from -1 to +1: +1 indicating an exact monotonic correlation, -1 an inverse monotonic correlation, and 0 no correlation. Its calculation is relatively simple and well implemented in python libraries as it is widely used in different research areas [15, 16]. In our example, $r_s = 909$ for Al and $r_s = 0.894$ for Fe which means a strong correlation between $I_d(t)$ and $S(t)$ on these videos. The mean values of r_s for all the videos of are shown in Table. 2 for both material. On average, $r_s = 0.717$ for aluminum, while for iron it goes up to 0.838.

Table 2 Average values of surface covered, maximum surface and spearman coefficient. Values are taken over 150 pulses for both Al and Fe.

Material	Al	Fe
Surface [mm^2]	0.727	0.479
Maximum surface [mm^2]	1.416	0.847
r_s	0.717	0.838

B. Current density

Once the surface and discharge current have been determined, it becomes interesting to calculate the evolution of the current density at the spots. Figure 5 shows the evolution of current density as a function of time on the videos exemplified in Fig. 3. This figure is obtained by dividing $I_d(t)$ by $S(t)$ (see Fig. 4). One can note 2 periods with high current density j at the beginning and the end of the discharge. Indeed, due to the identification method, uncertainty on the surface computation is large for these two instants. At the start, the spots are tightly grouped, regardless of the material. This tends to overestimate j because several spots are present per pixel. At the end of the discharge, the spots are scattered and not very bright. The optical arrangement of neutral density filters prevents these spots from being seen clearly, as their brightness falls below the threshold. This results in an underestimation of the surface area and, consequently, an overestimation of j. For aluminum, one point at 22 µs is outside the graph limits, while for iron, this overestimated point is around 0 µs.

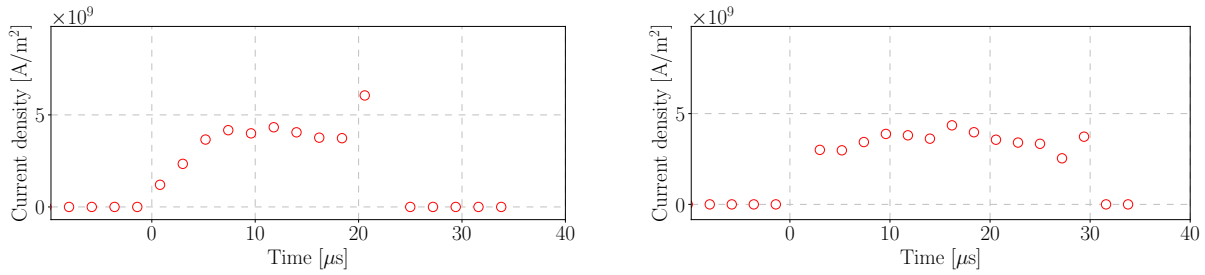

(a) Aluminum cathode, from video shown in Fig. 3a

(b) Iron cathode, from video shown in Fig. 3b

Fig. 5 Evolution of the current density during the discharge, for the two exemple videos.

If we disregard these 2 peaks, j remains stable around 4.5×10^9 A/m^2. The correlation between $I_d(t)$ and $S(t)$ has already been discussed in section V.A, it is then natural that current density should be relatively stable as current and surface evolve together. We can therefore calculate the average current density by taking the average current and dividing it by the average spot surface covered during the pulse. Results are given in table 3. It can be observed that the two materials have a fairly similar average current density, which is close to what has already been noted with other materials [14]. References in literature [17, 18] give a value of 5×10^9 A/m^2 according to the "large spot" model. This model predates the fractal spot model, developed in the early 2000s to better describe the cathode spot behavior [2, 4]. Here, because of the image resolution, the fractal model cannot be directly applied to our observations. Current density is then underestimated due to overestimation of the spot surface. In addition, direct observation of the cathode spots by optical means inherently overestimate their surface [19, 20]. The dense, rapidly expanding plasma from the spots can show a brightness almost equal to the one of the spot, within a certain radius. More recent studies suggest that the spot

current density would be closer to 10^{11} A/m^2, based on the ecton model[21] and advanced techniques such as pulsed laser absorption photography [22] or pulsed laser interferometry [23] .

Table 3 Average current density for the 2 materials.

Material	Al	Fe
Discharge current [A]	1.76×10^3	1.64×10^3
Spot current density [A/m^2]	2.42×10^9	3.42×10^9

Ultimately, the fractal model gives another perspective on the quest to determine the exact current density in cathode spots. They are self-similar and thus seem, with each new technological progress, to be composed of ever-smaller fragments. The question of the real spot current density is then still open and, in the end, is rather abstract.

C. Spot tracking and velocity

The propagation speed of the spots defines the capacity of the arc to erode the cathode. Combined with the observation of the evolution of the active spot surface, it gives important information on the dynamics of cathode erosion throughout a single PJP pulse. Implementing a tracking algorithm is quite complex here, given the random nature of spot motion and the low resolution of the image. However, successful results have been obtained with a modified particle tracking velocimetry (PTV) algorithm. PTV algorithms usually embed motion prediction models based on fluid mechanics physics in order to help the tracking from one frame to the other. Still, a reduced weight of this model on the detection algorithm allows to track semi-stochastic movement, with the condition of a fine tuning of the other tracking parameters. Here, we have specified an average spot size to search for, to aid spot detection. In doing so, we mainly track the bigger groups of spots and fewer spots are identified, reducing the number of detection errors. This choice was made to ease the tracking as the pictures are in gray-scale, the algorithm could therefore only analyze luminosity gradients and not the red-green-blue matrices.

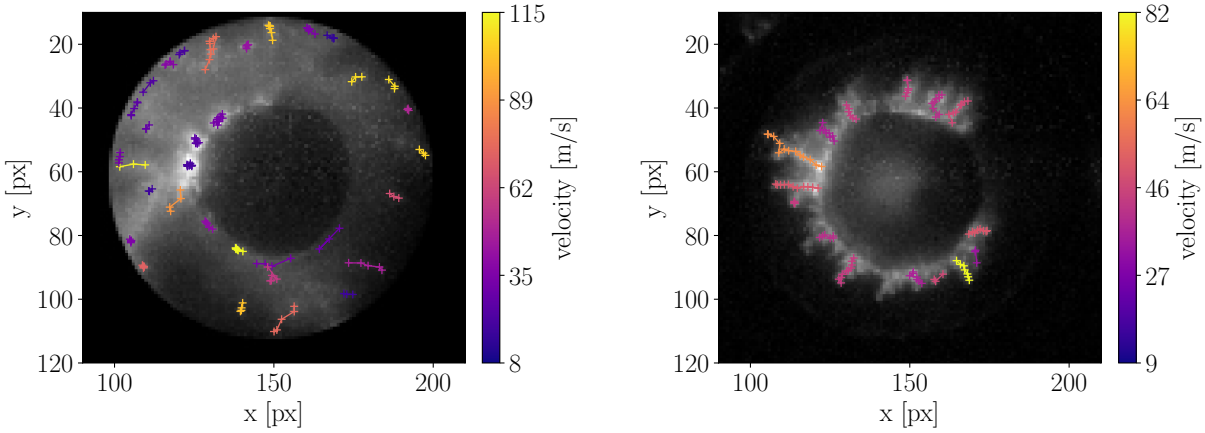

(a) Aluminum cathode, from video shown in Fig. 3a

(b) Iron cathode, from video shown in Fig. 3b

Fig. 6 Tracking of the spots on the two example videos.

Result of the tracking for the videos shown in Fig. 3 is shown in Fig. 6. The background picture is a sum of all the frames composing the video, making it analogous to a long-exposure photograph. The displayed lines are the trajectories of the different group of spots tracked on this video. Trajectories are colorized according to their respective average speed (norm of the velocity vector), the crosses symbolize the exact location where the spots have been identified. Despite the fact that trajectories can be either radial or tangential, it is observed that on iron, the trajectories are predominantly radial. In the example with aluminum, tracking is somewhat less precise for the reasons previously mentioned: smaller and dimmer spots. The trajectories in the aluminum figure include fewer points, which is a deliberate choice on our part. Given that the algorithm sometimes came short when it came to track the darker spots in the case of aluminum, the

tracking was intentionally stopped once a spot became difficult to identify. This was done to avoid errors and prevent a different spot from being mistakenly identified as part of the trajectory, which could artificially increase the calculated velocity. Additionally, low-velocity spots propagating along the edge of the cathode can be observed. This is due to the arc propagating on the cathode side in this example, which is a malfunctioning from the thruster in that case.

Finally, for both examples and thus for both materials, the trajectories remain relatively straight. This is somewhat surprising at first glance, considering that the spots are known to move in a random walk motion. Two possibilities can explain this observation. First, identifying groups of spots might lead to the observation of macroscopic effects, where the groups of spots propagate in relatively straight lines. This is quite consistent with the observations made by Hwangbo in reference [24]. By forcing the spots to cluster, it was noted both a decrease in the apparent velocity of the group and a less erratic propagation trajectory. Alternatively, it is possible that the camera's resolution is too low to capture the random walk, which likely occurs at the micrometer scale, essentially at the scale of a single pixel here [2, 14]. The famous "zigzag motion" [25] would thus be averaged, leaving only the main direction visible on the pictures.

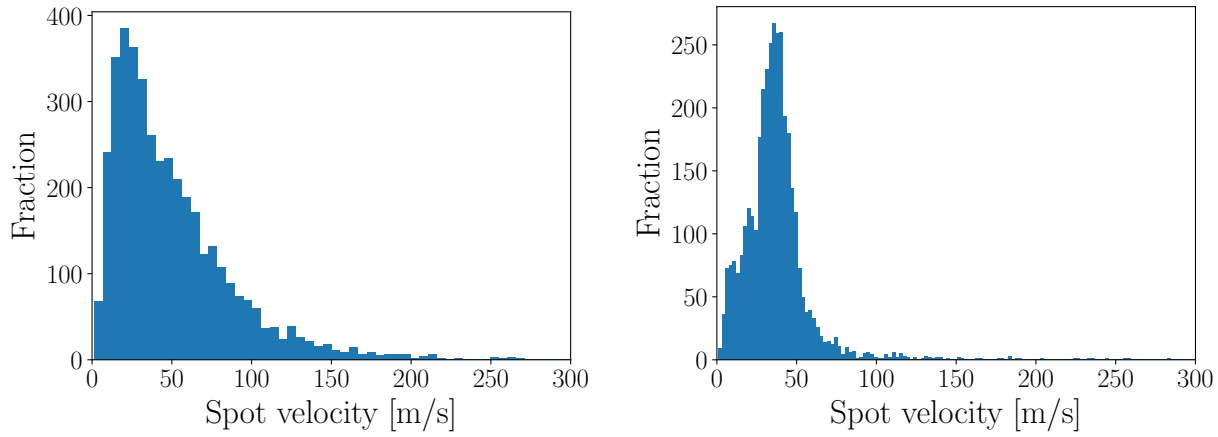

(a) Aluminum cathode

(b) Iron cathode

Fig. 7 Spot velocity distribution on the complete datasets, for the two materials.

Figure 7 shows the velocity distribution of all tracked spots across all discharges for each material, which represents approximately 4,000 trajectories in total per material. The average, median velocities, and standard deviations are provided in Table 4. The $\sigma_{\bar{v}}$ represents the standard deviation of the mean velocity over the pulses, while the σ_v represents the standard deviation across all tracked spots (i.e., the standard deviation of the histograms shown in Fig. 7). It can be observed that the statistical dispersion is significantly larger in the case of aluminum, which is partly due to greater uncertainty in spot detection and tracking.

However, this is not the only cause. We previously mentioned reference [24] in which the size of the spot clusters influences their propagation speed. Aluminum, in particular, exhibits smaller and more widely spaced spots, which are harder to track due to their lower brightness. Observations from the videos show that these types of spots are also faster, confirming both Hwangbo's results and the model by Kajita et al.,[24, 26]. The algorithm developed in our study is capable of tracking these spots when their size is not excessively small, as illustrated in Fig.,6a. The shorter, yellow trajectories, which correspond to the fastest spots, are linked to relatively dim regions in the summed image. By carefully observing the video (see Fig.,3a), it is evident that these are small spot clusters. These small, harder to detect clusters form the tail of the velocity distribution histogram, with velocities around 100 m/s.

The speeds presented here are higher than what is usually found in the literature [1, 27, 28]. Still, the PJP operates at a higher discharge current than the experimental arrangements used in these references. Specifically, the discharge current rate of rise $\dot{I_d}$ is notably higher in our experiment. Since the evolution of active spot surface increases linearly with current, and spots cannot ignite again after being active, the propagation speed of cathode spots is naturally linked to $\dot{I_d}$. Similar conclusions have been drawn by I. Beilis in ref. [27], with vacuum arcs under the influence of an external magnetic field.

Table 4 Average value of propagation velocity, median propagation velocity and associated standard deviations.

Material	Al	Fe
$\bar{v}$ [m/s]	49.3	37.5
$\sigma_{\bar{v}}$ [m/s]	10.4	7.2
med(v) [m/s]	38.5	35.4
σ_v [m/s]	39.2	23.4

D. Erosion

Observations regarding the spots dynamics can be linked to what is observed in terms of erosion. Figure 8a shows a comparison between a new (left) and a worn (right) titanium cathode operated for thousands of pulses. On the right cathode, it is clearly seen that a deep is forming close to the inside edge. The cathode is therefore not eroded evenly across its entire radius. The erosion profile is schematized in Fig. 8b. The area colorized in red represents the area of stronger erosion whereas the blue one represent the lower erosion. The fact that spots are initiated close to the central insulator and that tangential trajectories are observed underlies a higher probability density of spot ignition near the inner edge of the cathode. This naturally induce a stronger erosion in this area, which is remarked for all cathode material: the same pattern is observed for both aluminum and iron.

(a) Comparison between a new (left) and worn (right) titanium cathode.

(b) PJP cathode erosion map. The red area indicates a stronger erosion.

Fig. 8 Erosion profile on titanium cathodes.

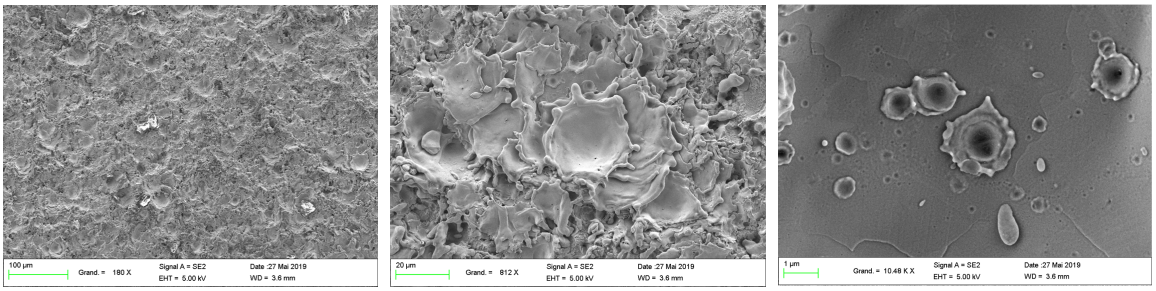

(a) 180x magnification

(b) 812x magnification

(c) 10480x magnification

Fig. 9 Microscope images of craters left on the cathode surface, for different magnifications (Cu cathode). Images provided by COMAT and reproduced with permission.

Figure 9 shows microscope images of the eroded section of a copper cathode (images provided by COMAT). In Fig. 9a, the surface condition of the cathode is clearly visible, appearing very granular with microprotrusions. These microprotrusions, small volumes of the cathode, are vaporized and ionized through an explosive process called ecton [7, 30]. Figure 9b provides a closer view of these marks, clearly revealing craters, the border of which indicate the liquid phase of the cathode spot [13, 31]. Meanwhile, Fig. 9c shows that each spot is actually composed of smaller

spots, fragments on the scale of tens of nanometers. This observation aligns with the conclusions drawn in Section V.B, demonstrating that this study focuses on the dynamics of spot clusters rather than individual spots.

VI. Conclusion

In this study, the behavior of cathode spots was investigated for two different cathode materials: aluminum and iron. For the same energy released in the discharge, aluminum and iron spots show very different dynamics. Aluminum spots exhibit faster propagation speeds, with greater dispersion in their velocity distribution. While it is challenging to discern a consistent behavior from one pulse to another, two main types of spots can be identified: large clusters propagating at around 40 m/s and smaller, spatially separated spots moving at approximately 100 m/s. The trajectories do not show a preferred direction, with spots spreading both radially and tangentially. In contrast, iron spots demonstrate a more predictable overall behavior, predominantly propagating radially outward from the center of the cathode.

However, despite these differing dynamics, the two materials show significant similarity in the instantaneous surface area covered by spots and the discharge current. When analyzing the statistical data instead of pulse-by-pulse behavior, a comparable current density is observed for both materials, approximately 5×10^9 A/m^2. This value can still be discussed due to the fractal nature of vacuum arc cathode spots, which makes it difficult to quantify the unit size of an emission cell. This study show the average behavior of a vacuum arc thruster, as a whole, taking data over many pulses. Accurate characterization of each pulse is a major challenge, due to the inherently stochastic nature of the vacuum arc. From an engineering standpoint, the outcome is quite clear: cathode erosion is concentrated primarily on the inner edge. This can limit the thruster lifetime, as the propellant is not optimally used across the entire cathode surface.

Acknowledgments

Authors would like to thank C. Chauveau and F. Halter for the high-speed camera as well as S. Iseni and M. Idir for the high quality optics. E. Michaux benefits from a CNES/COMAT PhD grant.

References

[1] Daalder, J., "Random walk of cathode arc spots in vacuum," *Journal of Physics D: Applied Physics*, Vol. 16, No. 1, 1983, p. 17. https://doi.org/10.1088/0022-3727/16/1/005.

[2] Anders, A., *Cathodic arcs: from fractal spots to energetic condensation*, Vol. 50, Springer, 2008. https://doi.org/10.1007/978-0-387-79108-1.

[3] Beilis, I., *Plasma and Spot Phenomena in Electrical Arcs*, Vol. 113, Springer Nature, 2020. https://doi.org/10.1007/978-3-030-44747-2.

[4] Anders, A., "The fractal nature of vacuum arc cathode spots," *IEEE Transactions on Plasma Science*, Vol. 33, No. 5, 2005, pp. 1456–1464. https://doi.org/10.1109/TPS.2005.856488.

[5] Anders, A., Oks, E., and Yushkov, G., "Cathodic arcs: Fractal voltage and cohesive energy rule," *Applied Physics Letters*, Vol. 86, No. 21, 2005, p. 211503. https://doi.org/10.1063/1.1937994.

[6] Blanchet, A., Herrero, L., Voisin, L., Pilloy, B., and Courteville, D., "Plasma Jet Pack Technology for Nano-Microsatellites," *36th International Electric Propulsion Conference*, 2019.

[7] Mesyats, G., "Ecton or electron avalanche from metal," *Physics-Uspekhi*, Vol. 38, No. 6, 1995, p. 567. https://doi.org/10.1070/PU1995v038n06ABEH000089.

[8] Michaux, E., Vinci, A., and Mazouffre, S., "Fractal dimension of cathode spots in a high-current vacuum arc thruster," *Vacuum*, 2023, p. 112286. https://doi.org/10.1016/j.vacuum.2023.112286.

[9] Oh, K., Kalanov, D., and Anders, A., "High-resolution observation of cathode spots in a magnetically steered vacuum arc plasma source," *Plasma Sources Science and Technology*, Vol. 30, No. 9, 2021, p. 095005. https://doi.org/10.1088/1361-6595/ac1ee1.

[10] Oh, K., Kalanov, D., Birtel, P., and Anders, A., "High-resolution observation of cathodic arc spots in a magnetically steered arc plasma source in low pressure argon, nitrogen, and oxygen atmospheres," *Journal of Applied Physics*, Vol. 130, No. 18, 2021, p. 183304. https://doi.org/10.1063/5.0072021.

[11] Golizadeh, M., Anders, A., Mendez Martin, F., Kolozsvári, S., and Franz, R., "Insights into surface modification and erosion of multi-element arc cathodes using a novel multilayer cathode design," *Journal of Applied Physics*, Vol. 127, No. 11, 2020, p. 113301. https://doi.org/10.1063/1.5141406.

[12] Juttner, B., "Nanosecond displacement times of arc cathode spots in vacuum," *IEEE transactions on plasma science*, Vol. 27, No. 4, 1999, pp. 836–844. https://doi.org/10.1109/27.782247.

[13] Beilis, I., "Vacuum arc cathode spot theory: history and evolution of the mechanisms," *IEEE Transactions on Plasma Science*, Vol. 47, No. 8, 2019, pp. 3412–3433. https://doi.org/10.1109/TPS.2019.2904324.

[14] Michaux, E., and Mazouffre, S., "High-speed imaging of cathode spots in a Vacuum Arc Thruster," *38th International Electric Propulsion Conference*, 2024, p. 291.

[15] Hauke, J., and Kossowski, T., "Comparison of values of Pearson's and Spearman's correlation coefficients on the same sets of data," *Quaestiones geographicae*, Vol. 30, No. 2, 2011, pp. 87–93. https://doi.org/10.2478/v10117-011-0021-1.

[16] De Winter, J., Gosling, S., and Potter, J., "Comparing the Pearson and Spearman correlation coefficients across distributions and sample sizes: A tutorial using simulations and empirical data." *Psychological methods*, Vol. 21, No. 3, 2016, p. 273. https://doi.org/10.1037/met0000079.

[17] Siemroth, P., Schulke, T., and Witke, T., "Investigation of cathode spots and plasma formation of vacuum arcs by high speed microscopy and spectroscopy," *IEEE Transactions on Plasma Science*, Vol. 25, No. 4, 1997, pp. 571–579. https://doi.org/10.1109/27.640667.

[18] Rakhovsky, V., "State of the art of physical models of vacuum arc cathode spots," *IEEE transactions on plasma science*, Vol. 15, No. 5, 1987, pp. 481–487. https://doi.org/10.1109/TPS.1987.4316741.

[19] Anders, S., Anders, A., and Juttner, B., "Brightness distribution and current density of vacuum arc cathode spots," *Journal of Physics D: Applied Physics*, Vol. 25, No. 11, 1992, p. 1591. https://doi.org/10.1088/0022-3727/25/11/005.

[20] Hantzsche, E., Juttner, B., and Ziegenhagen, G., "Why vacuum arc cathode spots can appear larger than they are," *IEEE transactions on plasma science*, Vol. 23, No. 1, 1995, pp. 55–64. https://doi.org/10.1109/27.376561.

[21] Mesyats, G., and Barengolts, S., "The cathode spot of a high-current vacuum arc as a multiecton phenomenon," *IEEE transactions on plasma science*, Vol. 29, No. 5, 2001, pp. 704–707. https://doi.org/10.1109/27.964458.

[22] Anders, A., Anders, S., Juttner, B., Botticher, W., Luck, H., and Schroder, G., "Pulsed dye laser diagnostics of vacuum arc cathode spots," *IEEE transactions on plasma science*, Vol. 20, No. 4, 1992, pp. 466–472. https://doi.org/10.1109/27.256775.

[23] Vogel, N., "The cathode spot plasma in low-current air and vacuum break arcs," *Journal of Physics D: Applied Physics*, Vol. 26, No. 10, 1993, p. 1655. https://doi.org/10.1088/0022-3727/26/10/017.

[24] Hwangbo, D., Kajita, S., Barengolts, S. A., Tsventoukh, M. M., and Ohno, N., "Transition in velocity and grouping of arc spot on different nanostructured tungsten electrodes," *Results in Physics*, Vol. 4, 2014, pp. 33–39. https://doi.org/10.1016/j.rinp.2014.03.001.

[25] Jüttner, B., and Kleberg, I., "The retrograde motion of arc cathode spots in vacuum," *Journal of Physics D: Applied Physics*, Vol. 33, No. 16, 2000, p. 2025. https://doi.org/10.1088/0022-3727/33/16/315.

[26] Kajita, S., Hwangbo, D., Ohno, N., Tsventoukh, M. M., and Barengolts, S. A., "Arc spot grouping: An entanglement of arc spot cells," *Journal of Applied Physics*, Vol. 116, No. 23, 2014. https://doi.org/10.1063/1.4904917.

[27] Beilis, I., Sagi, B., Zhitomirsky, V., and Boxman, R., "Cathode spot motion in a vacuum arc with a long roof-shaped cathode under magnetic field," *Journal of Applied Physics*, Vol. 117, No. 23, 2015. https://doi.org/10.1063/1.4922862.

[28] Chaly, A., Logatchev, A., and Shkol'nik, S., "Cathode spot dynamics on pure metals and composite materials in high-current vacuum arcs," *IEEE Transactions on Plasma Science*, Vol. 25, No. 4, 1997, pp. 564–570. https://doi.org/10.1109/27.640666.

[29] Barengolts, S., Mesyats, G., and Shmelev, D., "Structure and time behavior of vacuum arc cathode spots," *IEEE transactions on plasma science*, Vol. 31, No. 5, 2003, pp. 809–816. https://doi.org/10.1109/TPS.2003.818449.

[30] Mesyats, G., "Cathode Phenomena in a Vacuum Discharge: The Breakdown, the Spark and the Arc," Nauka, 2000, p. 400.

[31] Beilis, I., "The vacuum arc cathode spot and plasma jet: Physical model and mathematical description," *Contributions to Plasma Physics*, Vol. 43, No. 3-4, 2003, pp. 224–236.